Neurotoxicity Research (2019) 36:724–735
https://doi.org/10.1007/s12640-019-00068-0

ORIGINAL ARTICLE

Diffusion Kurtosis Imaging Detects Microstructural Changes in a Methamphetamine-Induced Mouse Model of Parkinson's Disease

Anas Arab[1] · Jana Ruda-Kucerova[1] · Alzbeta Minsterova[2,3] · Eva Drazanova[1,4] · Nikoletta Szabó[5,6] · Zenon Starcuk Jr[4] · Irena Rektorova[2] · Amit Khairnar[2,7]

Received: 22 October 2018 / Revised: 24 May 2019 / Accepted: 28 May 2019 / Published online: 18 June 2019

Abstract

Methamphetamine (METH) abuse is known to increase the risk of Parkinson's disease (PD) due to its dopaminergic neurotoxicity. This is the rationale for the METH model of PD developed by toxic METH dosing (10 mg/kg four times every 2 h) which features robust neurodegeneration and typical motor impairment in mice. In this study, we used diffusion kurtosis imaging to reveal microstructural brain changes caused by METH-induced neurodegeneration. The METH-treated mice and saline-treated controls underwent diffusion kurtosis imaging scanning using the Bruker Avance 9.4 Tesla MRI system at two time-points: 5 days and 1 month to capture both early and late changes induced by METH. At 5 days, we found a decrease in kurtosis in substantia nigra, striatum and sensorimotor cortex, which is likely to indicate loss of DAergic neurons. At 1 month, we found an increase of kurtosis in striatum and sensorimotor cortex and hippocampus, which may reflect certain recovery processes. Furthermore, we performed tract-based spatial statistics analysis in the white matter and at 1 month, we observed increased kurtosis in ventral nucleus of the lateral lemniscus and some of the lateral thalamic nuclei. No changes were present at the early stage. This study confirms the ability of diffusion kurtosis imaging to detect microstructural pathological processes in both grey and white matter in the METH model of PD. The exact mechanisms underlying the kurtosis changes remain to be elucidated but kurtosis seems to be a valuable biomarker for tracking microstructural brain changes in PD and potentially other neurodegenerative disorders.

Keywords Behaviour · Diffusion kurtosis imaging · Methamphetamine · Mice · MRI · Parkinson's disease · Tract-based spatial statistics

✉ Jana Ruda-Kucerova
jkucer@med.muni.cz

[1] Department of Pharmacology, Faculty of Medicine, Masaryk University, Kamenice 5, 625 00 Brno, Czech Republic

[2] Applied Neuroscience Research Group, CEITEC - Central European Institute of Technology, Masaryk University, Brno, Czech Republic

[3] Faculty of Medicine, Masaryk University, Brno, Czech Republic

[4] Institute of Scientific Instruments of the Czech Academy of Sciences, Brno, Czech Republic

[5] Department of Neurology, Faculty of Medicine, Albert Szent-Györgyi Clinical Centre, University of Szeged, Szeged, Hungary

[6] Central European Institute of Technology CEITEC, Neuroscience Centre, Masaryk University, Brno, Czech Republic

[7] Department of Pharmacology and Toxicology, National Institute of Pharmaceutical Education and Research (NIPER), Ahmedabad, Gandhinagar, Gujrat, India

Introduction

Parkinson's disease (PD) is one of the most common progressive neurodegenerative disorders, characterized by the loss of 50–70% of dopaminergic (DAergic) neurons in substantia nigra (SN). DAergic neurodegeneration leads to motor symptoms represented typically by bradykinesia, resting tremor, muscle rigidity and gait problems (Chaudhuri and Martinez-Martin 2008). Although the aetiology of PD and the exact mechanisms responsible for neuronal loss remain to be elucidated, it has been postulated that many factors such as ageing, environmental toxins, genetic predisposition and neuroinflammation contribute to the development of PD (Costa and Caltagirone 2015). Other mechanisms such as oxidative stress, the rise of iron content and pathological protein accumulation are also likely to play a role in the pathology (Prakash et al. 2016; Rizek et al. 2016). Neuroinflammation is a reaction of the innate immune system within central

nerves system to infections, trauma, toxins and other stimuli, which leads to activation of resident immune cells (microglia and astroglia) and release of pro-inflammatory mediators (Kreutzberg 1996; Pan et al. 2010). This acute neuroinflammatory response may trigger oxidative and nitrosative stress, that is short-lived and unlikely to be detrimental to long-term neuronal survival (Frank-Cannon et al. 2009). In contrast, chronic neuroinflammation includes not only longstanding activation of microglia and subsequent sustained release of inflammatory mediators but also results in increased oxidative and nitrosative stress, which may lead to neurodegeneration (Tansey et al. 2007).

Methamphetamine (METH) abuse studies proved that METH intake might lead to the development of neurodegenerative disorders, such as PD (Tavassoly and Lee 2012). METH intoxication causes an elevation of intracellular inclusions similar to Lewy bodies in PD, which feature the presence of ubiquitin and α-synuclein, and it also leads to accumulation of α-synuclein in SN (Fornai et al. 2005). Postmortem human studies reported that neurotoxic processes continue for more than 7 days up until 1 month after METH administration, and induce reduction in the dopamine (DA) content, tyrosine hydroxylase expression, and DA transporter binding in the striatum of METH abusers (Lappin et al. 2018). Similarly, preclinical studies showed that an acute exposure to neurotoxic METH doses leads to decreases in DA content in the cortex and striatum, hippocampus and amygdala (Achat-Mendes et al. 2005; Bowyer et al. 2008; Fantegrossi et al. 2008). Furthermore, METH was shown to increase the neuronal apoptosis in the striatum, frontal and parietal cortices, hippocampus and olfactory bulb (Cadet et al. 2005; Cunha-Oliveira et al. 2008). Importantly, METH plays a role in the activation of astrocytosis and microgliosis, and it triggers the release of pro-inflammatory cytokines leading to glial dysfunction and neuronal death (Thomas and Kuhn 2005; Zhu et al. 2006; Bowyer et al. 2008; Fantegrossi et al. 2008; Moratalla et al. 2017). These neurotoxic effects persist up to 1 month and induce time-dependent microstructural changes of the brain tissue (Moratalla et al. 2017).

These changes may be tracked in vivo by structural neuroimaging methods, such as diffusion tensor imaging (DTI), which was recently applied in the diagnosis of several neurodegenerative diseases (Rovaris and Filippi 2007; Rolheiser et al. 2011). DTI provides a unique information in characterizing tissue microstructure (Basser 1995; Basser 1997). Using two main parameters: mean diffusivity (MD), which is a directionally averaged measure of diffusion, and fractional anisotropy (FA), which is a measure of the directionality of diffusion (Pierpaoli et al. 1996). Several clinical studies have demonstrated that DTI could detect the changes in white matter (WM) of PD patients at both early and late stage of PD (Vaillancourt et al. 2009; Schwarz et al. 2013; Knossalla et al. 2018). However, the applicability of DTI is limited by the inherent assumptions that the voxels are internally homogeneous and that water diffusion in brain is sufficiently characterized as Gaussian. Such a model of diffusion is well-proven for bulk water but does not sufficiently reflect the complexity of biological systems. This limits the ability of DTI to accurately detect the diffusion parameters in heterogeneous biological tissues and their change due to disease. For instance, DTI fails to detect crossing or diverging WM fibres, in which diffusion may appear as isotropic due to the model inability to describe the overlay of several anisotropic diffusion components in the same voxel. This restriction is based on the fact that while neuron dimensions range mostly between 1 and 20 μm, the MRI voxel size is much larger, typically 50–500 μm. Moreover, DTI is also not able to map the non-Gaussian diffusion found in spatially restricted compartments. Whereas in white matter (WM), diffusion is highly anisotropic and mostly properly reflected by DTI, DTI is not truly effective in detecting changes in grey matter (GM), which is nearly isotropic. On the other hand, it may be significant how much diffusion is restricted, i.e. non-Gaussian, in GM (Jensen and Helpern 2010; Arab et al. 2018). Therefore, diffusion kurtosis imaging (DKI), which is an extension of DTI, was developed to assess non-Gaussian diffusion and characterize the diffusional heterogeneity of the brain tissue. Moreover, both the apparent diffusion coefficient and apparent diffusion kurtosis can be obtained by DKI, which provides a second-order approximation of water displacement distribution. Kurtosis is a dimensionless measure of the degree of diffusion hindrance or restriction and reflects the changes in structural complexity (Jensen and Helpern 2010; Hansen and Jespersen 2017; Arab et al. 2018). Recent clinical studies utilizing DKI proved its ability to differentiate between PD patients and control subjects. According to most of these studies, the increase or decrease in DKI can be caused by different factors, e.g. the increase in DKI may be explained by pathological protein accumulation or iron deposition while the decrease in DKI may indicate neuronal loss (Wang et al. 2011; Kamagata et al. 2014; Kamagata et al. 2017).

Despite the potential usefulness of DKI in PD research, only a few preclinical studies have employed this method. In our earlier studies, we observed kurtosis and diffusivity changes using DKI in TNWT-61 transgenic mouse model of PD (Khairnar et al. 2015; Khairnar et al. 2016; Khairnar et al. 2017). However, this animal model features a robust accumulation of human α-synuclein, but it does not show any neurodegeneration (Delenclos et al. 2014).

Therefore, this study aimed to expand the knowledge about DKI sensitivity to a different model of PD, which reflects the neurodegenerative features of human PD. We employed a

previously validated neurotoxic METH treatment and evaluated the phenotype at 5 days and 1 month time-points after METH dosing. In this PD-like model, METH administration damages DAergic fibres in the striatum and their cell bodies in the SN and it partially mimics the neurodegeneration pattern observed in human patients (Sonsalla et al. 1996; Natale et al. 2008; Ares-Santos et al. 2012; Granado et al. 2013). To confirm the behavioural validity of the model, we also evaluated motor impairment by standard behavioural tests.

Material and Methods

Animals

Seventy-one male C57BL/6 mice12–14 weeks old were obtained from the Masaryk University breeding facility (Brno, Czech Republic). The mice were group housed in standard rodent polycarbonate cages, ($n = 10$) per cage. Then, the animals were randomly assigned to the methamphetamine (METH)-treated and control (saline—SAL-treated) group. A behavioural study was performed with METH ($n = 20$) and SAL ($n = 20$) treated animals. One half of each group was subjected to a battery of motor tests on day 5 and the other half on day 30 in order to avoid habituation effect in the tests. For the MRI study, METH ($n = 20$) and SAL ($n = 11$) treated mice were transported to the animal house of the Institute of Scientific Instruments of the Czech Academy of Sciences, Brno, and maintained under the same conditions as in the previous location. Neuroimaging was performed on two separate groups of METH and SAL at 5 days and 1 month time-point: at 5 days, METH ($n = 11$) and SAL ($n = 5$) and at 1 month, METH ($n = 9$) and SAL ($n = 6$). The behavioural and MRI studies were performed in separate groups of animals, as these methods could not be combined in one laboratory.

Environmental conditions during the whole study were constant: relative humidity 50–60%, room temperature 23 °C ± 1 °C, regular 12-h light-dark cycle (6 a.m. to 6 p.m. darkness). Food and water were available ad libitum. All procedures were performed in accordance with EU Directive no. 2010/63/EU and approved by the Animal Care Committee of the Faculty of Medicine, Masaryk University, Czech Republic and Czech Governmental Animal Care Committee, in compliance with Czech Animal Protection Act No. 246/1992.

Drugs and Treatments

Methamphetamine (METH, Sigma Chemical, Co., St Louis, MO, USA) was dissolved in sterile saline to a concentration of 10 mg in 10 ml. The solution was administered intraperitoneally at a dose of 10 mg/kg on day 1 of the study at 4 separate doses every 2 h (Sonsalla et al. 1996).

Behavioural Profile

Challenging Beam Traversal Test (CBW) Motor performance was measured with a challenging beam traversal test (Fleming et al. 2004, 2006; Schintu et al. 2009). Briefly, the mice were trained to traverse a 1-m non-reflective grey hardened polyvinyl chloride (PVC) beam consisting of four sections (25 cm each) with different widths (3.5 to 0.5 cm by 1 cm decrements) leading to the mice's home cage. After a day of training, a mesh grid (1 cm squares) of the corresponding width was placed over the beam surface, leaving approximately a 1 cm space between the grid and the beam surface. The mice were then videotaped while traversing the grid-surfaced beam for three trials. Videotapes were manually scored in slow motion for the number of slips and the time to traverse across three trials by an experienced investigator blind to the mouse genotype. Scores were calculated across all three trials and averaged for each mouse.

Square and Round Beam Walk Tests (SBW, RBW) The beam walk tests were set up as described in a previous study (Suidan et al. 2013), the mice transversed two 1 m beams raised approximately 50 cm above the surface: the first beam was 10 mm wide and square, the second beam was 16 mm wide and round. To motivate the mice to cross the beam to the home cage, which was placed at the end of the beam, each mouse was placed on the far end of the beam and allowed to cross to the home cage once.

Grid Test The inverted grid test was used to assess neuromuscular abnormalities. Mice were placed in the centre of a horizontal square (12 × 12 cm) grid consisting of wire mesh (mesh loop of 0.5 cm^2) surrounded by non-reflective grey hardened PVC walls. The grid was placed 20 cm above a table-top and was rotated upside down, allowing the mouse to move freely. The test was performed by inverting the grid. The latency to fall off the grid was recorded with a maximum cutoff duration of 60 s (Tillerson and Miller 2003; Fleming et al. 2004; Sgado et al. 2011).

Pole Test The test has been used to assess basal ganglia-related movement disorders in mice (Fleming et al. 2006; Schintu et al. 2009). Briefly, the animals were placed head-up on top of a vertical wooden pole covered by mull (diameter 8 mm, height 55 cm). When placed on the pole, animals turned downward and descended the length of the pole back into the home cage. Mice were subjected to training a day before the test, which consisted of three trials. On the test day, animals had three trials, and the total time to orient downward (t-turn) and descend the pole was measured with a maximum cutoff duration of 120 s.

Diffusion-Weighted MR Data Acquisition

DKI data were obtained with a Bruker Avance 9.4 T MRI system equipped with a gradient system delivering up to 660 mT/m. All experiments were performed using a quadrature volume transmit coil (inner diameter 86 mm) and a four-channel surface phased array receive head coil. Mice were anaesthetised using isoflurane inhalation (1.5–2%) and monitored to maintain constant physiological parameters. Fast low angle shot (FLASH) scout images were used to localize the bregma position. Reference T2-weighted brain scans were acquired using the 2D RARE (rapid acquisition with relaxation enhancement) sequence with the following acquisition parameters: 24 × 24 mm field of view (FOV), 256 × 256 acquisition matrix size, and 15 adjacent slices of 0.5-mm slice thickness. RARE factor of 8 was employed and the repetition time (TR) was 2500 ms with four averages for a total acquisition time of ~ 6 min. For the DKI acquisition, diffusion-weighted images were acquired with two-shot spin-echo echo-planar imaging (SE-EPI). Respiratory gating was used to prevent motion artefacts. The generalized autocalibrating partially parallel acquisitions (GRAPPA) with an acceleration factor of 2 was used to improve image quality by reducing sensitivity to motion and inhomogeneity of magnetic susceptibility. The DKI protocol included the acquisition of six b-values ($b = 0$, 500, 1000, 1500, 2000 and 2500 s/mm^2) along with 30 non-collinear directions, $\delta = 4$ ms, $\Delta = 11$ ms, with seven averages used for $b = 0$ acquisition and four averages for each other b value. The maximal b value 2500 s/mm^2 was proved to be the optimal setting for the WM in DKI model, but some authors claim that this b value may cause an underestimation in calculation of DKI parameters in GM (Chuhutin et al. 2017). The SE-EPI pulse sequence (FOV = 24 × 24 mm, acquisition matrix = 98 × 128, echo time TE = 25 ms using 300 kHz bandwidth and TR ~ 5 s depending on respiratory rate) was used to produce images of 15 adjacent slices (0.5-mm thickness) within a total acquisition time of approximately 100 min. The maps in this study reflect DTI and DKI metrics: axial diffusivity (AD), radial diffusivity (RD) and mean diffusivity (MD), which reflect different diffusion directionality. AD measures the extent of diffusion occurring in the direction parallel with the fibre. RD reflects the extent of diffusion occurring in directions perpendicular to the fibre (Alexander et al. 2000; Alexander et al. 2007) and MD is a mean value of diffusion in all directions. Kurtosis metrics: axial kurtosis (AK), radial kurtosis (RK) and mean kurtosis (MK) have the similar meanings, respectively.

Data Analysis

MRI data were converted to NIfTI from the Bruker format with a Matlab script programmed locally. Diffusion data were corrected for eddy currents and motion artefacts to the first non-diffusion-weighted image (Jenkinson and Smith, 2001). The following parametric maps were calculated in ExploreDTI v4.8.4. Software (Leemans and Jones 2009): MK, AK, RK, MD, AD, RD and FA, using the robust estimation of tensors by outlier rejection (RESTORE) fitting method. For further data analysis, two different approaches were applied:

A. Region of interest (ROI) analysis

Averaged diffusion, FA and kurtosis parameters were obtained from multiple regions: the SN (one slice), striatum (average of four slices), sensorimotor cortex (average of five slices), hippocampus (average of three slices) and thalamus (average of two slices). We chose these specific ROIs based on published histology results showing a substantial accumulation of α-synuclein in these brain areas (Chesselet et al. 2012) and on our previous studies with 9 months and 14 months TNWT-61 mice (Khairnar et al. 2015; Khairnar et al. 2016). The ROI selection in $b = 0$ images was drawn manually according to the mouse brain atlas (Franklin and Paxinos 2013) with the help of FA maps using ImageJ® software for various brain regions. The delineations of the ROIs are shown in Fig. 1.

B. Tract-based spatial statistics (TBSS)

WM analysis was performed using the TBSS algorithm (Smith et al. 2006) in FSL. Automatic brain extraction was carried out with BET (Smith 2002); brain-extracted maps were checked one by one visually and the extraction was corrected manually. TBSS was implemented and modified according to the protocol for rodent brains (Sierra et al. 2011). All the data were firstly affine-registered into common 3D space in order to make the comparison of affected WM tracts easier. Then the TBSS was used with following steps: (1) co-registration of all individual FA maps and identification of the best registration target with the free-search method, (2) application of the best registration target as a template for final transformations, (3) calculation of the mean FA map and creation of the mean FA skeleton at the threshold of 0.2 that represents the core of all tracts, (4) projection of each mouse's FA data to this skeleton and (5) repetition of the previous steps for all DKI maps. Since changes were expected only in well-circumscribed regions of the WM, it would have been over-conservative to correct for multiple correlations based on the total number of voxels in the skeleton. Hence, we used the non-corrected statistics threshold at the 1% significance level. Only clusters larger than 4 voxels were considered for further analysis and discussion (Csete et al. 2014). The results of the TBSS analysis were identified according the mouse brain atlas (Franklin and Paxinos 2013).

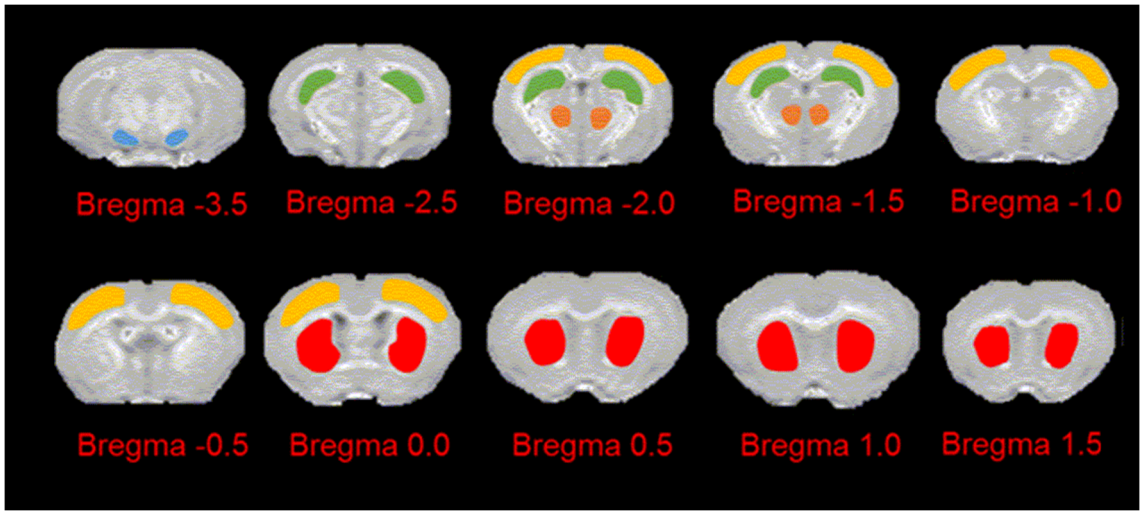

Fig. 1 Delineation of ROIs: hippocampus, sensorimotor cortex, striatum, substantia nigra and thalamus according to the Paxinos Mouse Brain Atlas overlaid on mean kurtosis maps (slice thickness 500 μm). In the majority of the ROIs, more slices were analysed; the number is indicated in brackets. Colour codes: substantia nigra: blue (1 slice), hippocampus: green (3 slices), sensorimotor cortex: yellow (5 slices), striatum: red (4 slices), thalamus: orange (2 slices)

Statistical Data Analysis

Both behavioural and MRI data were expressed as arithmetic mean ± SEM. The effect of the PD model (METH vs. SAL) was tested in all behavioural tasks, DKI and TBSS parameters using either a two sample unpaired Student's *t* test when the data passed the Kolmogorov–Smirnov normality test or Mann–Whitney *U* test when the data were non-parametric (non-parametric variables were the following: 5 days MK and RK in substantia nigra, 1 month MK in hippocampus, RD in substantia nigra and FA in striatum). The level of statistical significance was set at $p < 0.05$, and the results are supplemented with 95% confidence intervals for mean differences in all cases. This is by nature an exploratory study using a several ROIs and numerous DKI variables to reveal the most useful measures. However, this approach greatly increases the number of comparisons. Therefore, in the statistical analysis, we opted for presentation of non-corrected results and accept a risk of potentially false positive results in order to reveal potentially important differences in specific ROIs and DKI metrics. Medical relevance of our data will need to be carefully confirmed by clinical studies in the future.

Results

5-Day Time-Point

Behavioural Tests

The results of the motor performance tests showed a trend of motor impairment. METH-treated animals made significantly more slips in RBW test [*t* test, $p = 0.026$; CI (− 4.418, − 0.316)], CBW test [*t* test, $p = 0.040$; CI (− 1.755, − 0.045)] and in the grid test, latency to fall showed a trend [*t* test, $p = 0.061$, CI (− 0.339, 13.509)] as compared to SAL. All 5-day time-point behavioural data are summarized in Fig. 2.

ROI MRI

ROI analysis of the DKI variables showed lower of MK and RK in SN (MWU test, $p = 0.007$, $p = 0.009$ respectively), together with lower MK in the STR and cortex [*t* test, $p = 0.006$; CI (0.018, 0.009) and $p = 0.034$; CI (0.003, 0.056) respectively] in the METH-treated animals as compared to SAL. In contrast, METH-treated animals exhibited higher RD in SN [*t* test, $p = 0.045$; CI (− 0.0002, − 0.0000002)] and higher AD in the cortex [*t* test, $p = 0.048$; CI (− 0.0002, − 0.000001)] compared to SAL. All 5-day MRI data are summarized in Fig. 3.

TBSS MRI

The TBSS analysis was performed in the same animals in order to examine changes in WM in METH- and SAL-treated animals. There was no significant difference between the two groups.

1-Month Time-Point

Behavioural Tests

The results of the motor performance tests showed a moderate motor impairment in the METH-treated animals at 1-month time-point. Specifically, METH-treated animals took more time in SBW test [*t* test, $p = 0.044$; CI (− 3.192, − 0.044)],

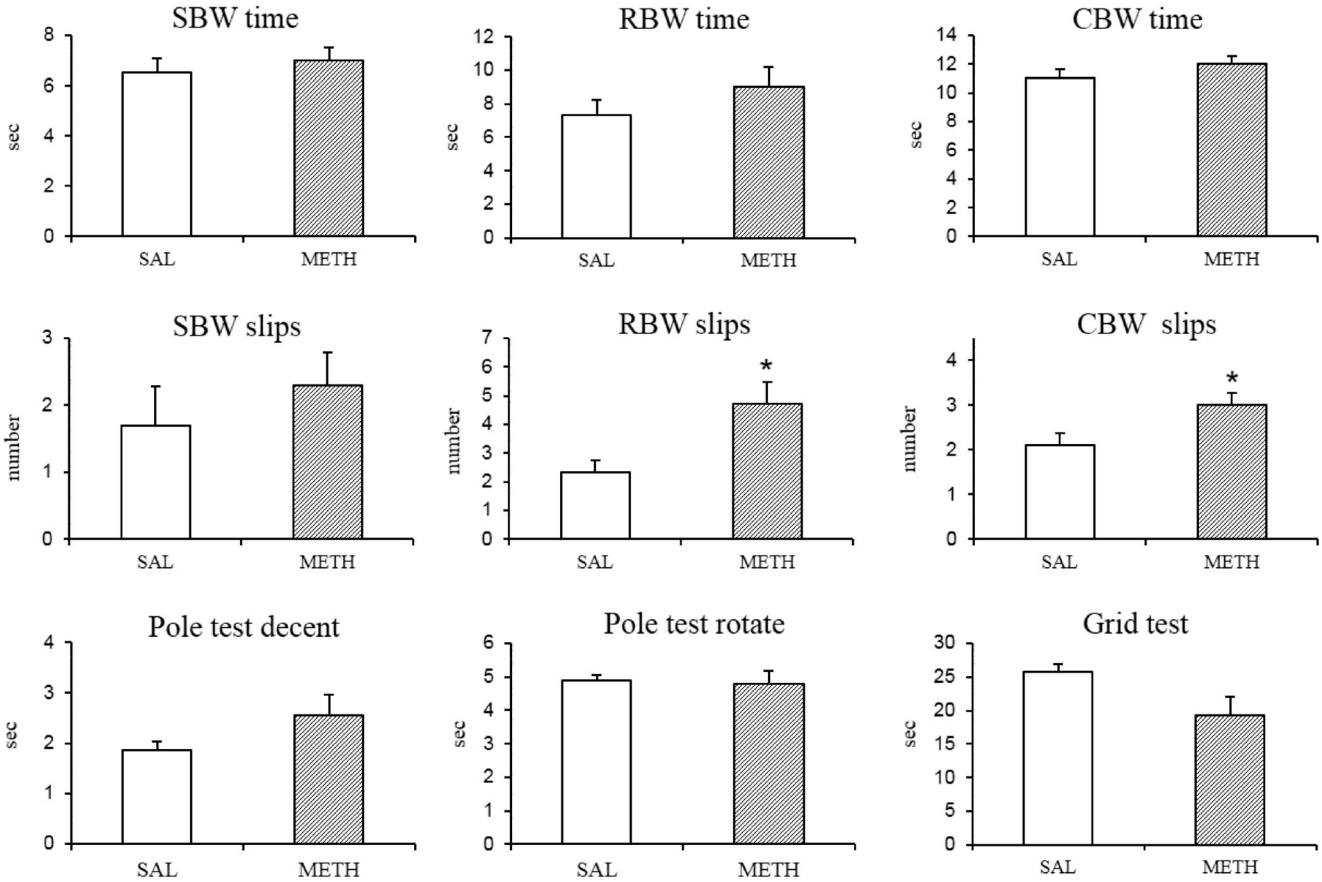

Fig. 2 Behaviour at 5-day time-point. The bar graphs represent motor performance in METH- and SAL-treated mice at 5-day time-point. Data are expressed as mean values ±SEM, *$p < 0.05$. SBW square beam walk, RBW round beam walk, and CBW challenging beam walk test

CBW test [t test, $p < 0.001$; CI (− 8.626, − 5.234)] and in pole test [time to rotate, t test, $p = 0.003$; CI (− 5.436, − 1.290)] as compared to SAL. The latency to fall in the grid test was significantly shorter in METH-treated animals [t test, $p < 0.001$; CI (5.123, 14.506)] as compared to SAL. All 1-month behavioural data are summarized in Fig. 4.

ROI MRI

ROI analysis revealed that METH-treated animals showed higher MK in STR, cortex and hippocampus [t test, $p = 0.038$; CI (− 0.076, − 0.003), t test, $p = 0.048$; CI (− 0.048, − 0.0002), MWU test, $p = 0.013$, respectively] and MK showed a trend in SN [t test, $p = 0.052$; CI (− 0.075, 0.0004)] in METH-treated animals as compared to SAL. In the DTI parameters, METH-treated animals showed lower MD in hippocampus and STR [t test, $p = 0.044$; CI (0.000003, 0.0002), $p = 0.047$; CI (0.000002, 0.0002) respectively], and lower RD in SN [t test, $p = 0.018$; CI (0.00002, 0.0002)] in METH-treated animals as compared to SAL. FA was found to be higher in the cortex, hippocampus, SN and STR [t test, $p = 0.036$; CI (− 0.028, − 0.001), t test, $p = 0.034$; CI (− 0.020, − 0.0009), t test, $p = 0.011$; CI (− 0.048, − 0.007), and MWU test, $p = 0.0177$ respectively] in METH-treated animals as compared to SAL. All 1-month time-point MRI data are summarized in Fig. 5.

TBSS MRI

In the WM, there was a higher FA unilaterally in the primary somatosensory cortex, fornix and ventral nucleus of the lateral lemniscus [t test, $p = 0.0046$; CI (0.283, 0.530)] in METH-treated animals. RK was also found to be higher unilaterally in ventral nucleus of the lateral lemniscus and some of the lateral thalamic nuclei [t test, $p = 0.0031$; CI (1.395, 1.901)]. On the contrary, the MD was lower in METH-treated animals, in cingulum, external capsule and some of the lateral thalamic nuclei [t test, $p < 0.001$; CI (0.002, 0.006)]. Lower AD was found in the cingulate cortex and external capsule [t test, $p = 0.0031$; CI (0.002, 0.006)] in METH-treated animals. Furthermore, lower RD was observed in cingulum, primary somatosensory cortex, external capsule, some of the lateral thalamic nuclei and ventral nucleus of the lateral lemniscus [t test, $p = 0.0031$; CI (0.001, 0.003)] in METH-treated animals. No differences were found in MK and AK. The data are summarized in Fig. 6.

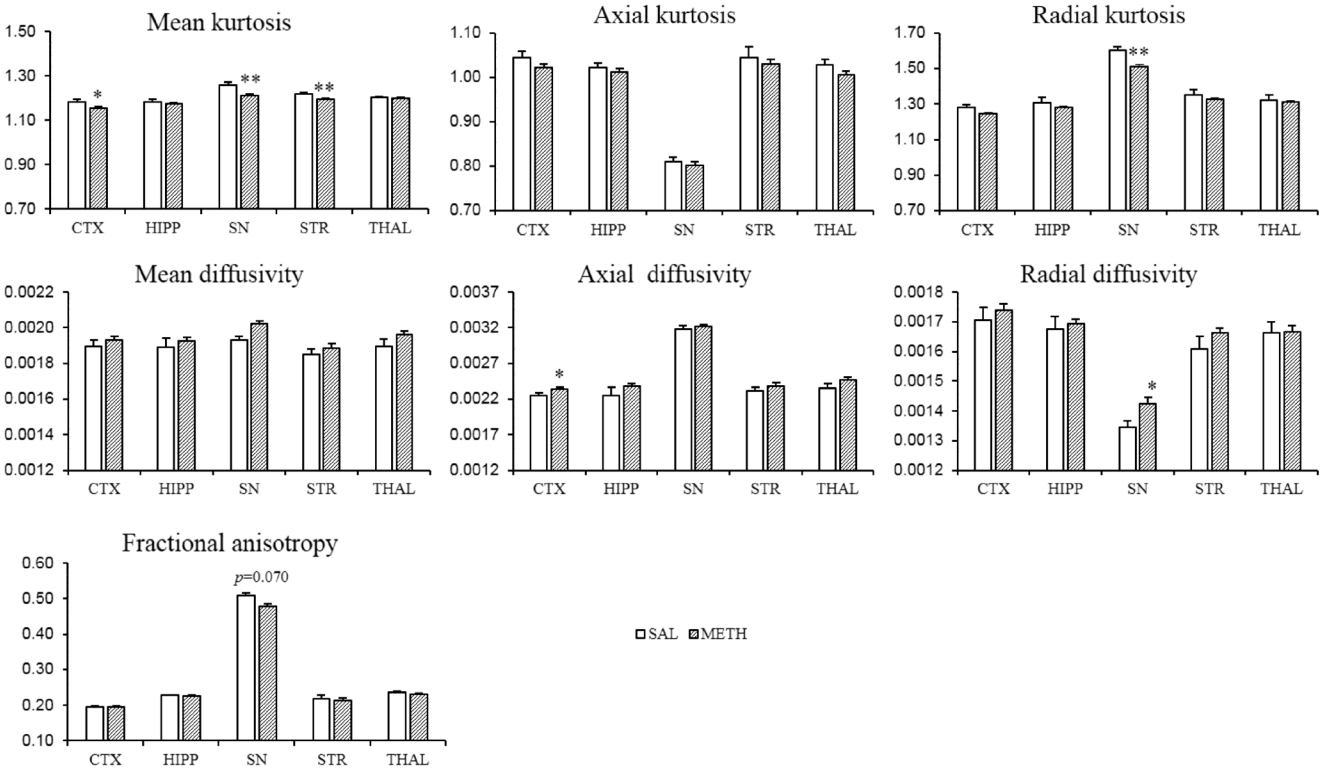

Fig. 3 DKI ROI analysis at 5-day time-point. Bar graphs represent DKI parameters in METH and SAL-treated mice at 5-day time-point. Data are expressed as mean ± SEM, $*p < 0.05$, $**p < 0.01$. Kurtosis and fractional anisotropy are dimensionless units; diffusivity values are given in mm^2/s. In order to make the changes in DKI variables visible, the *y*-axis does not start at zero. CTX sensorimotor cortex, HIPP hippocampus, SN substantia nigra, STR striatum, THAL thalamus

Discussion

In this study, METH-treated animals showed moderate motor impairment at different behavioural traits assessing motor performance. These behavioural results provide evidence of dysfunction of the nigrostriatal system and are in line with our previous reports using a genetic model of PD (Khairnar et al. 2015; Khairnar et al. 2016; Khairnar et al. 2017). These data support the validity of PD-like phenotype development of this animal model in this study.

The primary aim of this study was to perform DKI imaging to assess the microstructural changes induced by METH treatment. We used ROI-based analysis to detect changes in the GM; the regions were selected based on our previous research using TNWT-61 transgenic model of PD: sensorimotor cortex, hippocampus, STR, SN and thalamus (Khairnar et al. 2015; Khairnar et al. 2016; Khairnar et al. 2017). TBSS analysis was also used to assess the WM at two different time-points, at 5 days and 1 month after METH treatment. In both types of analysis, we found significant changes in kurtosis and diffusivity metrics in METH-treated animals as compared to SAL-treated control groups.

It has been consistently reported that administration of neurotoxic doses of METH in rodents induces selective loss of DAergic axon terminals in STR along with decrease in level of DA and its metabolites as well as DAergic cell body loss in SN (Granado et al. 2010; Ares-Santos et al. 2012). The loss of DA signalling in these areas underlie the prompt development of PD-like behavioural phenotype (Walsh and Wagner 1992; Tieu 2011). The ROI-based analysis in this study revealed a decrease of MK at 5-day time-point in SN, STR and sensorimotor cortex in METH-treated animals. At this early time-point, MK was the most sensitive readout of METH-induced changes.

There are not many reports regarding potential cortical damage induced by METH in either clinical or animal studies. Previous structural imaging studies in METH abusers reported structural alterations in the cortico-striatal pathway. It has been reported that METH users exhibit smaller cortical and larger striatal volumes than non-users (Berman et al. 2008). Furthermore, it has been reported that METH treatment induces degeneration of cortical neurons both in clinical (Kuehn 2011; Hsieh et al. 2014) and animal studies (Commins and Seiden 1986). Our isolated findings in the sensorimotor cortex may be in line with the evidence and may reflect neurodegenerative changes in the cortex.

On the other hand, at the late 1-month time-point, both MK and FA showed consistent results opposite to the 5-day time-point. Specifically, both MK and FA values were increased in sensorimotor cortex, hippocampus, SN and STR. Lower MD

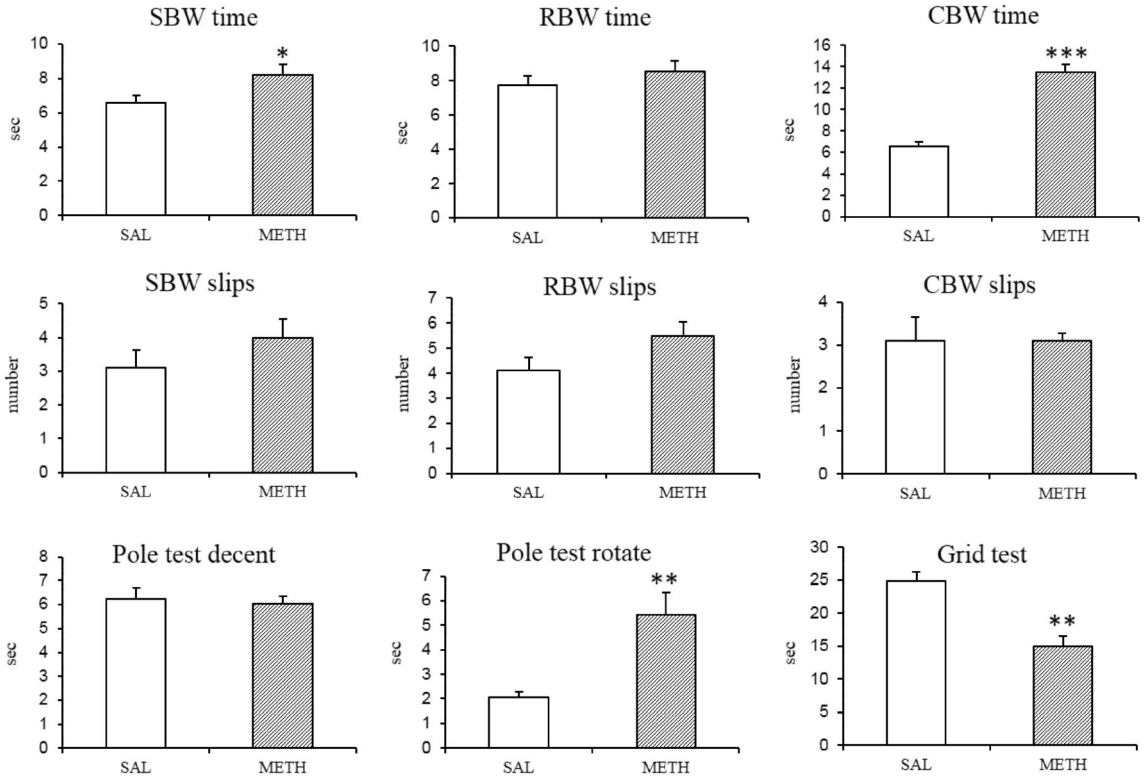

Fig. 4 Behaviour at 1-month time-point. The bar graphs represent motor performance in METH- and SAL-treated mice at 1-month. Data are expressed as mean values ±SEM, *$p < 0.05$, **$p < 0.01$, ***$p < 0.001$. SBW square beam walk, RBW round beam walk, and CBW challenging beam walk test

in hippocampus and STR may support the findings we observed by MK and FA in the same regions. The axial and radial variables (both kurtosis and diffusivity) did not show any patterns at either time-point. An intriguing issue is the opposite direction of the DKI metrics at the two time-points. At 5 days, DKI metrics detected more isotropic tissue microstructure in the METH-treated mice while at 1-month, the data indicate increased diffusion hindrance. This may be explained either by potential recovery from the METH-induced insult, or protein accumulation.

Specific recovery phenomenon for the striatal and SN DA system has already been reported in animal studies after METH neurotoxic doses treatment (Granado et al. 2013). This recovery pattern has been attributed to the regeneration of nerve terminal and/or compensatory collateral sprouting from residual terminals (Harvey et al. 2000). Khan et al. 2016 recently reported increase in MK and decrease in MD in amygdala of stressed rats due to increase in neurite density in stressed rats as compare to control rats. They also mentioned that increase in neurite density may have increased non-Gaussanity in the extracellular space of amygdala in stressed rats (Khan et al. 2016). Similarly, in our METH model, we have found increase in MK and decrease in MD in the hippocampus and striatum, which might be coming from neuronal sprouting as a recovery phenomenon. Neurotoxic METH administration downregulates DA transporters (DAT), which influence DA signalling in both human abusers (Volkow et al. 2015) and animals (Fleckenstein et al. 1997). DAT number was shown to recover as soon as 24 h after acute METH treatment in rats (Fleckenstein et al. 1997). However, it is unclear if the loss of DAT after METH treatment reflects the damage of DAergic neurons and whether normalization of DAT number may indicate their regeneration (Volkow et al. 2001; Volkow et al. 2015).

Protein accumulation may also explain the increased kurtosis metrics in the late time-points in this study. It was shown that neurotoxic METH treatment in mice induces intracellular inclusions similar to Lewy bodies in PD, which feature the presence of ubiquitin and α-synuclein (Fornai et al. 2005). Furthermore, an in vitro study in PC12 cells exposed to METH has observed increased expression of α-synuclein along with nitric oxide synthase and nitric oxide claiming involvement of S-nitrosylation of protein disulphide isomerase α-synuclein accumulation (Wu et al. 2014). Similarly, another study on rats exposed to METH found an epigenetic link in increasing expression of α-synuclein (Jiang et al. 2014). Therefore, the opposite DKI results observed here might be due to the increased expression of α-synuclein and other intracellular inclusions, which also supports the validity of this animal model of PD.

In our previous studies, we have reported a robust effect of α-synuclein accumulation on MK using the TNWT-61 transgenic model of PD in mice. This transgenic model allows

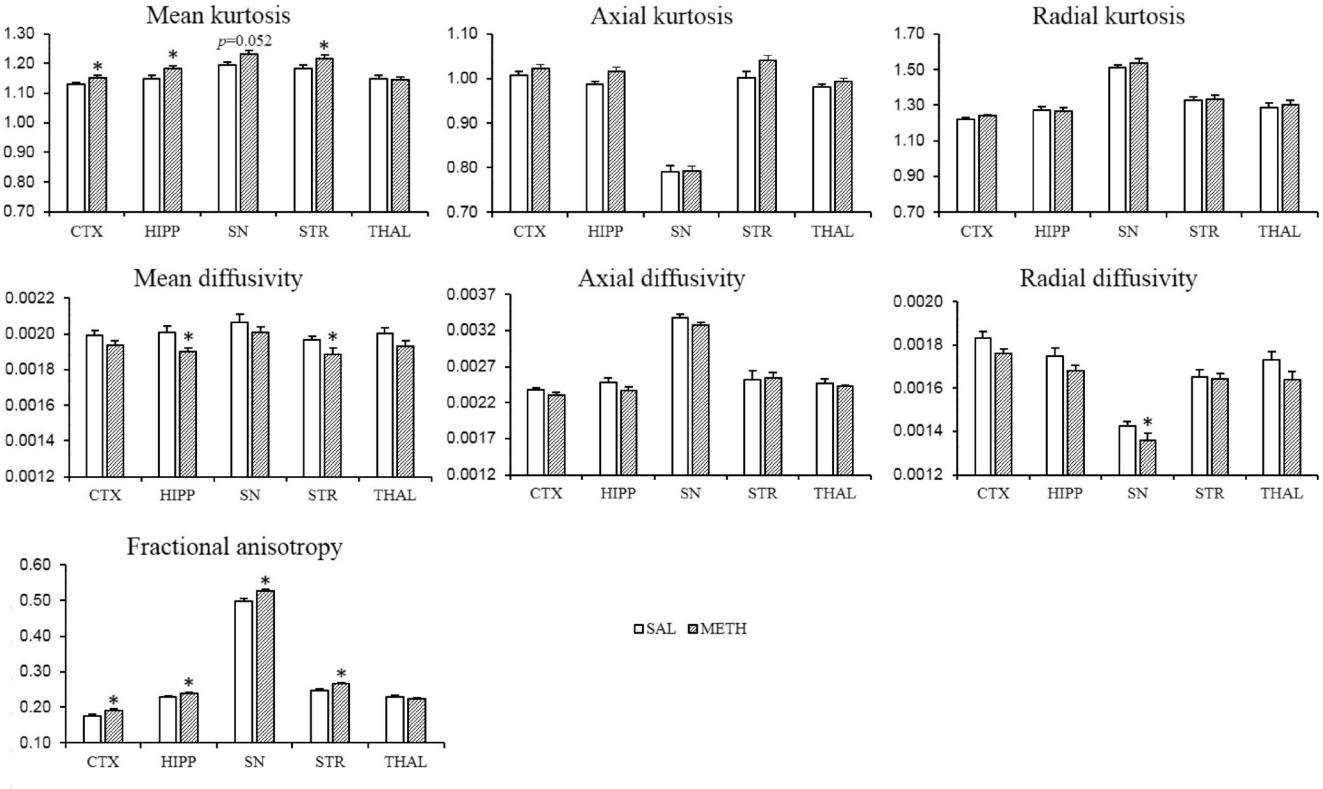

Fig. 5 DKI ROI analysis at 1-month time-point. Bar graphs represent DKI parameters in METH- and SAL-treated mice at 1-month time-point. Data are expressed as mean ± SEM, $*p < 0.05$. Kurtosis and fractional anisotropy are dimensionless units; diffusivity values are given in mm^2/s. In order to make the changes in DKI variables visible, the *y*-axis does not start at zero. CTX sensorimotor cortex, HIPP hippocampus, SN substantia nigra, STR striatum, THAL thalamus

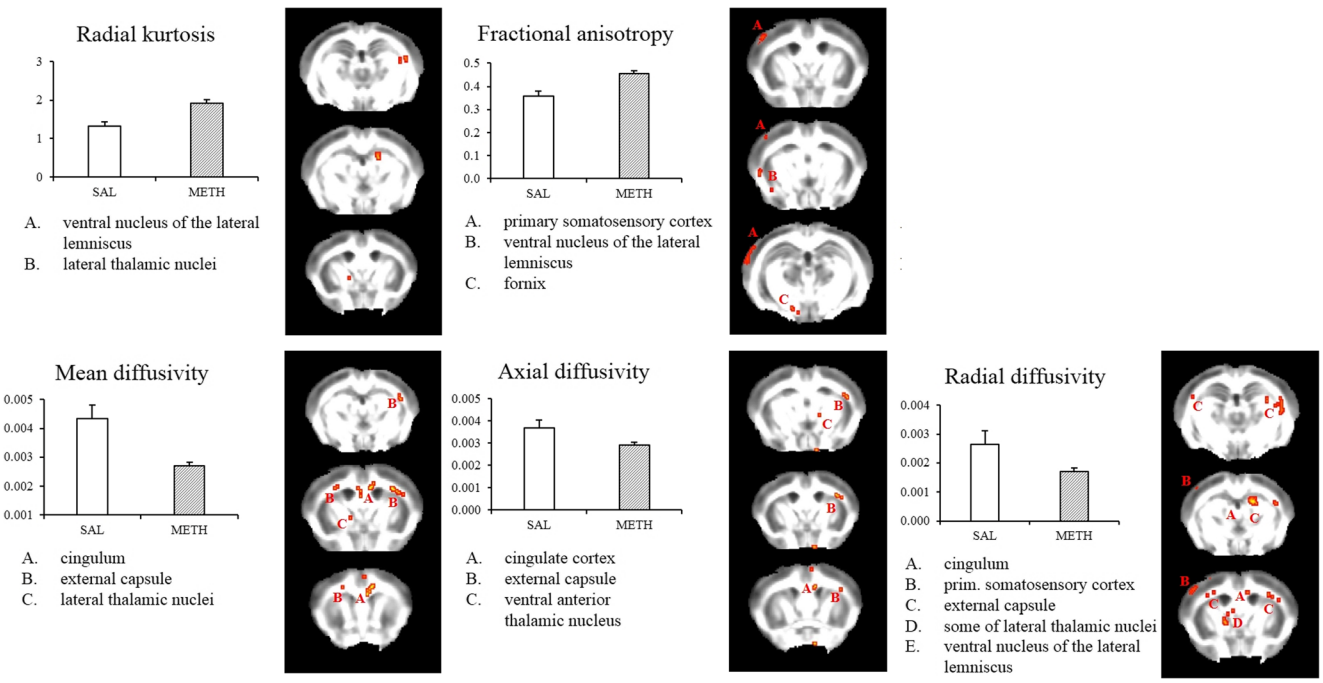

Fig. 6 TBSS analysis at 1-month time-point. Bar graphs represent averaged TBSS parameters under the altered regions. All presented changes are significant with $p < 0.01$ on uncorrected data, cluster with 5 and more voxels. Data are expressed as mean values ±SEM. No significant changes were observed in MK and AK

discrete evaluation of effects caused by the α-synuclein pathology. We have consistently observed increase of MK in TNWT-61 mice in a growing number of ROIs: from STR and thalamus at 3 months of age to STR, SN, sensorimotor cortex, thalamus and hippocampus at 14 months of age (Khairnar et al. 2015; Khairnar et al. 2016; Khairnar et al. 2017). Interestingly, there is a large agreement between MK results observed in the late time-point of this study and the data obtained in the TNWT-61 mice at 9 and 14 months of age (Khairnar et al. 2015; Khairnar et al. 2016). Specifically, the STR, SN and sensorimotor cortex exhibit increase of MK in both models. This supports the pathological protein accumulation as a critical underlying process leading to the increase of MK observed in the late time-point of this study.

On the other hand, thalamus was unaffected in either time-point in this study while our studies using TNWT-61 mice at the age of 3 to 14 months reported thalamus as one of the first ROIs showing changes in the DKI metrics (Khairnar et al. 2015; Khairnar et al. 2016; Khairnar et al. 2017). This discrepancy between the two models of PD is likely due to a completely different nature of these models. The TNWT-61 mice lack any neurodegeneration, and they feature mainly human α-synuclein expression (Khairnar et al. 2015; Khairnar et al. 2016; Khairnar et al. 2017), while the METH treatment is mainly neurotoxic and α-synuclein inclusions are formed during the neurodegenerative process (Fornai et al. 2005).

With the help of TBSS analysis, we were able to detect significant differences of several WM regions in METH-treated animals as compared to SAL-treated controls, only at the 1-month time-point. The changes in the DKI metrics are consistent throughout all WM regions, e.g. an increase of RK and FA occurs together with a decrease of diffusivity variables (MD, RD and RD), that is an indication of water-molecule mobility restriction such as due to neuronal sprouting, glial cell activation or protein accumulation (Khairnar et al. 2016; Arab et al. 2018). This may indicate a consistent microstructural impairment in the WM due to the neurotoxic METH exposure. Similarly, WM hypertrophy has been reported in chronic METH abusers and it might be due to neuronal adaptation, cell death, adaptive glial proliferation or altered myelination (London et al. 2004; Thompson et al. 2004). Taken together, in our model the microstructure of WM seems to be intact at the early time-point while in the late stage, it seems to be widely affected.

Conclusion

In summary, this study shows the sensitivity of DKI in the detection of microstructural changes triggered by neurotoxic METH treatment in the GM. We have detected opposite results in the early and late time-point of the study. This may be explained by a rapid neurodegenerative and neuroinflammatory response at the beginning—reflected by a decrease of MK, and protein accumulation following after1 month—leading to an increase of MK. The most sensitive readout of GM in this study was MK, which was able to differentiate between METH-treated animals and SAL. This goes in line with our previous transgenic animal model studies, where MK was also the most sensitive DKI parameter altered by alpha synuclein accumulation (Khairnar et al. 2015; Khairnar et al. 2016; Khairnar et al. 2017). Therefore, DKI may become a biomarker able to selectively detect different microstructural pathological processes in the brain. However, additional experiments need to be performed to elaborate and confirm the findings of this exploratory study, more PD-like animal models should be tested, and the exact nature of mechanisms underlying the MK changes should be comprehensively evaluated.

Acknowledgments The authors are grateful to Dr. Peter Latta for his valuable technical support and help with the MRI scanning and a professional data analyst Ms. Daniela Kuruczova for her advice on statistical analysis. The behavioural apparatuses for the challenging beam traversal and grid test were kindly provided by Jiri Kucera, Environmental Measuring Systems, Brno, Czech Republic.

Funding This study was performed at Masaryk University as part of the project "Pharmacological research in the field of pharmacokinetics, neuropsychopharmacology and oncology", number MUNI/A/1550/2018, with the support of the Specific University Research Grant, as provided by the Ministry of Education, Youth and Sports of the Czech Republic in the year 2019 and also supported by funds from the Faculty of Medicine MU to junior researcher Jana Ruda-Kucerova. The work was also supported from European Regional Development Fund-Project "National infrastructure for biological and medical imaging" (No. CZ.02.1.01/0.0/0.0/16_013/0001775). We acknowledge the core facility MAFIL of CEITEC and the MR unit and the animal facility (CZ62760225) of ISI CAS, both supported by the Czech-BioImaging large RI project (LM2015062 funded by MEYS CR), for their support with obtaining scientific data presented in this paper. Nikoletta Szabo was supported by NAP 2.0 (2017-1.2.1-NKP-2017-00002), EFOP-3.6.1-16-2016-00008 and KTIA_13_NAP-A-II/20. The ISI CAS support was further co-financed by MEYS CR and EC (CZ.1.05/2.1.00/01.0017) and by the CAS (RVO:68081731).

Compliance with Ethical Standards

Conflict of Interest The authors declare that they have no conflict of interest.

References

Achat-Mendes C, Ali SF, Itzhak Y (2005) Differential effects of amphetamines-induced neurotoxicity on appetitive and aversive Pavlovian conditioning in mice. Neuropsychopharmacology 30(6): 1128–1137

Alexander AL, Hasan K, Kindlmann G, Parker DL, Tsuruda JS (2000) A geometric analysis of diffusion tensor measurements of the human brain. Magn Reson Med 44(2):283–291

Alexander AL, Lee JE, Lazar M, Field AS (2007) Diffusion tensor imaging of the brain. Neurotherapeutics 4(3):316–329

Arab A, Wojna-Pelczar A, Khairnar A, Szabó N, Ruda-Kucerova J (2018) Principles of diffusion kurtosis imaging and its role in early diagnosis of neurodegenerative disorders. Brain Res Bull 139:91–98

Ares-Santos S, Granado N, Oliva I, O'Shea E, Martin ED, Colado MI, Moratalla R (2012) Dopamine D (1) receptor deletion strongly reduces neurotoxic effects of methamphetamine. Neurobiol Dis 45(2): 810–820

Basser PJ (1995) Inferring microstructural features and the physiological state of tissues from diffusion-weighted images. NMR Biomed 8(7–8):333–344

Basser PJ (1997) New histological and physiological stains derived from diffusion-tensor MR images. Ann N Y Acad Sci 820:123–138

Berman S, O'Neill J, Fears S, Bartzokis G, London ED (2008) Abuse of amphetamines and structural abnormalities in the brain. Ann N Y Acad Sci 1141:195–220

Bowyer JF, Thomas M, Schmued LC, Ali SF (2008) Brain region-specific neurodegenerative profiles showing the relative importance of amphetamine dose, hyperthermia, seizures, and the blood-brain barrier. Ann N Y Acad Sci 1139:127–139

Cadet JL, Jayanthi S, Deng X (2005) Methamphetamine-induced neuronal apoptosis involves the activation of multiple death pathways. Review. Neurotox Res 8(3–4):199–206

Chaudhuri KR, Martinez-Martin P (2008) Quantitation of non-motor symptoms in Parkinson's disease. Eur J Neurol 15(Suppl 2):2–7

Chesselet MF, Richter F, Zhu C, Magen I, Watson MB, Subramaniam SR (2012) A progressive mouse model of Parkinson's disease: the Thy1-aSyn ("line 61") mice. Neurotherapeutics 9(2):297–314

Chuhutin A, Hansen B, Jespersen SN (2017) Precision and accuracy of diffusion kurtosis estimation and the influence of b-value selection. NMR Biomed 30(11):e3777

Commins DL, Seiden LS (1986) Alpha-methyltyrosine blocks methylamphetamine-induced degeneration in the rat somatosensory cortex. Brain Res 365(1):15–20

Costa A, Caltagirone C (2015) Individual differences in approach-avoidance aptitude: some clues from research on Parkinson's disease. Front Syst Neurosci 9:43

Csete G, Szabo N et al (2014) An investigation of the white matter microstructure in motion detection using diffusion MRI. Brain Res 1570:35–42

Cunha-Oliveira T, Rego AC, Oliveira CR (2008) Cellular and molecular mechanisms involved in the neurotoxicity of opioid and psychostimulant drugs. Brain Res Rev 58(1):192–208

Delenclos M, Carrascal L, Jensen K, Romero-Ramos M (2014) Immunolocalization of human alpha-Synuclein in the Thy1-aSyn ("line 61") transgenic mouse line. Neuroscience 277:647–664

Fantegrossi WE, Ciullo JR, Wakabayashi KT, de la Garza R II, Traynor JR, Woods JH (2008) A comparison of the physiological, behavioral, neurochemical and microglial effects of methamphetamine and 3, 4-methylenedioxymethamphetamine in the mouse. Neuroscience 151(2):533–543

Fleckenstein AE, Metzger RR, Wilkins DG, Gibb JW, Hanson GR (1997) Rapid and reversible effects of methamphetamine on dopamine transporters. J Pharmacol Exp Ther 282(2):834–838

Fleming SM, Salcedo J, Fernagut PO, Rockenstein E, Masliah E, Levine MS, Chesselet MF (2004) Early and progressive sensorimotor anomalies in mice overexpressing wild-type human alpha-Synuclein. J Neurosci 24(42):9434–9440

Fleming SM, Salcedo J, Hutson CB, Rockenstein E, Masliah E, Levine MS, Chesselet MF (2006) Behavioral effects of dopaminergic agonists in transgenic mice overexpressing human wildtype alpha-Synuclein. Neuroscience 142(4):1245–1253

Fornai F, Lenzi P, Ferrucci M, Lazzeri G, Poggio AB, Natale G, Busceti CL, Biagioni F, Giusiani M, Ruggieri S, Paparelli A (2005) Occurrence of neuronal inclusions combined with increased nigral expression of alpha-Synuclein within dopaminergic neurons following treatment with amphetamine derivatives in mice. Brain Res Bull 65(5):405–413

Frank-Cannon TC, Alto LT, McAlpine FE, Tansey MG (2009) Does neuroinflammation fan the flame in neurodegenerative diseases? Mol Neurodegener 4:47

Franklin, K. B. J. and G. Paxinos (2013). Paxinos and Franklin's the mouse brain in stereotaxic coordinates

Granado N, Ares-Santos S, O'Shea E, Vicario-Abejón C, Colado MI, Moratalla R (2010) Selective vulnerability in striosomes and in the nigrostriatal dopaminergic pathway after methamphetamine administration: early loss of TH in striosomes after methamphetamine. Neurotox Res 18(1):48–58

Granado N, Ares-Santos S et al (2013) Methamphetamine and Parkinson's disease. Parkinsons Dis 2013:308052

Hansen B, Jespersen SN (2017) Recent developments in fast kurtosis imaging. Front Phys 5(40)

Harvey DC, Lacan G, Tanious SP, Melega WP (2000) Recovery from methamphetamine induced long-term nigrostriatal dopaminergic deficits without substantia nigra cell loss. Brain Res 871(2):259–270

Hsieh JH, Stein DJ et al (2014) The neurobiology of methamphetamine induced psychosis. Front Hum Neurosci 8:537

Jenkinson, M., Smith, S., 2001. A global optimisation method for robust affineregistration of brain images. Med. Image Anal. 5, 143–156.

Jensen JH, Helpern JA (2010) MRI quantification of non-Gaussian water diffusion by kurtosis analysis. NMR Biomed 23(7):698–710

Jiang W, Li J, Zhang Z, Wang H, Wang Z (2014) Epigenetic upregulation of alpha-Synuclein in the rats exposed to methamphetamine. Eur J Pharmacol 745:243–248

Kamagata K, Tomiyama H, Hatano T, Motoi Y, Abe O, Shimoji K, Kamiya K, Suzuki M, Hori M, Yoshida M, Hattori N, Aoki S (2014) A preliminary diffusional kurtosis imaging study of Parkinson disease: comparison with conventional diffusion tensor imaging. Neuroradiology 56(3):251–258

Kamagata, K., A. Zalesky, et al. (2017). "Gray matter abnormalities in idiopathic Parkinson's disease: evaluation by diffusional kurtosis imaging and neurite orientation dispersion and density imaging." Hum Brain Mapp

Khairnar A, Latta P, Drazanova E, Ruda-Kucerova J, Szabó N, Arab A, Hutter-Paier B, Havas D, Windisch M, Sulcova A, Starcuk Z, Rektorova I (2015) Diffusion kurtosis imaging detects microstructural alterations in brain of alpha-Synuclein overexpressing transgenic mouse model of Parkinson's disease: a pilot study. Neurotox Res 28(4):281–289

Khairnar A, Ruda-Kucerova J, Drazanova E, Szabó N, Latta P, Arab A, Hutter-Paier B, Havas D, Windisch M, Sulcova A, Starcuk Z Jr, Király A, Rektorova I (2016) Late-stage alpha-Synuclein accumulation in TNWT-61 mouse model of Parkinson's disease detected by diffusion kurtosis imaging. J Neurochem 136(6):1259–1269

Khairnar A, Ruda-Kucerova J, Szabó N, Drazanova E, Arab A, Hutter-Paier B, Neddens J, Latta P, Starcuk Z Jr, Rektorova I (2017) Early and progressive microstructural brain changes in mice overexpressing human alpha-Synuclein detected by diffusion kurtosis imaging. Brain Behav Immun 61:197–208

Khan AR, Chuhutin A, Wiborg O, Kroenke CD, Nyengaard JR, Hansen B, Jespersen SN (2016) Biophysical modeling of high field diffusion MRI demonstrates micro-structural aberration in chronic mild stress rat brain. Neuroimage 142:421–430

Knossalla F, Kohl Z, Winkler J, Schwab S, Schenk T, Engelhorn T, Doerfler A, Gölitz P (2018) High-resolution diffusion tensor-imaging indicates asymmetric microstructural disorganization within substantia nigra in early Parkinson's disease. J Clin Neurosci 50:199–202

Kreutzberg GW (1996) Microglia: a sensor for pathological events in the CNS. Trends Neurosci 19(8):312–318

Kuehn BM (2011) Meth use linked to risk of Parkinson disease. JAMA 306(8):814

Lappin JM, Darke S, Farrell M (2018) Methamphetamine use and future risk for Parkinson's disease: evidence and clinical implications. Drug Alcohol Depend 187:134–140

Leemans A, Jones DK (2009) The B-matrix must be rotated when correcting for subject motion in DTI data. Magn Reson Med 61(6):1336–1349

London ED, Simon SL, Berman SM, Mandelkern MA, Lichtman AM, Bramen J, Shinn AK, Miotto K, Learn J, Dong Y, Matochik JA, Kurian V, Newton T, Woods R, Rawson R, Ling W (2004) Mood disturbances and regional cerebral metabolic abnormalities in recently abstinent methamphetamine abusers. Arch Gen Psychiatry 61(1):73–84

Moratalla R, Khairnar A, Simola N, Granado N, García-Montes JR, Porceddu PF, Tizabi Y, Costa G, Morelli M (2017) Amphetamine-related drugs neurotoxicity in humans and in experimental animals: main mechanisms. Prog Neurobiol 155:149–170

Natale G, Kastsiuchenka O, Pasquali L, Ruggieri S, Paparelli A, Fornai F (2008) MPTP- but not methamphetamine-induced parkinsonism extends to catecholamine neurons in the gut. Ann N Y Acad Sci 1139:345–349

Pan MH, Lai CS, Ho CT (2010) Anti-inflammatory activity of natural dietary flavonoids. Food Funct 1(1):15–31

Pierpaoli C, Jezzard P, Basser PJ, Barnett A, di Chiro G (1996) Diffusion tensor MR imaging of the human brain. Radiology 201(3):637–648

Prakash KG, Bannur BM, Chavan MD, Saniya K, Sailesh KS, Rajagopalan A (2016) Neuroanatomical changes in Parkinson's disease in relation to cognition: an update. J Adv Pharm Technol Res 7(4):123–126

Rizek P, Kumar N, Jog MS (2016) An update on the diagnosis and treatment of Parkinson disease. CMAJ 188(16):1157–1165

Rolheiser TM, Fulton HG, Good KP, Fisk JD, McKelvey JR, Scherfler C, Khan NM, Leslie RA, Robertson HA (2011) Diffusion tensor imaging and olfactory identification testing in early-stage Parkinson's disease. J Neurol 258(7):1254–1260

Rovaris M, Filippi M (2007) Diffusion tensor MRI in multiple sclerosis. J Neuroimaging 17(Suppl 1):27S–30S

Schintu N, Frau L, Ibba M, Garau A, Carboni E, Carta AR (2009) Progressive dopaminergic degeneration in the chronic MPTPp mouse model of Parkinson's disease. Neurotox Res 16(2):127–139

Schwarz ST, Abaei M, Gontu V, Morgan PS, Bajaj N, Auer DP (2013) Diffusion tensor imaging of nigral degeneration in Parkinson's disease: a region-of-interest and voxel-based study at 3 T and systematic review with meta-analysis. Neuroimage Clin 3:481–488

Sgado P, Viaggi C et al (2011) Behavioral, neurochemical, and electrophysiological changes in an early spontaneous mouse model of nigrostriatal degeneration. Neurotox Res 20(2):170–181

Sierra A, Laitinen T, Lehtimäki K, Rieppo L, Pitkänen A, Gröhn O (2011) Diffusion tensor MRI with tract-based spatial statistics and histology reveals undiscovered lesioned areas in kainate model of epilepsy in rat. Brain Struct Funct 216(2):123–135

Smith SM (2002) Fast robust automated brain extraction. Hum Brain Mapp 17(3):143–155

Smith SM, Jenkinson M, Johansen-Berg H, Rueckert D, Nichols TE, Mackay CE, Watkins KE, Ciccarelli O, Cader MZ, Matthews PM, Behrens TEJ (2006) Tract-based spatial statistics: voxelwise analysis of multi-subject diffusion data. Neuroimage 31(4):1487–1505

Sonsalla PK, Jochnowitz ND, Zeevalk GD, Oostveen JA, Hall ED (1996) Treatment of mice with methamphetamine produces cell loss in the substantia nigra. Brain Res 738(1):172–175

Suidan GL, Duerschmied D, Dillon GM, Vanderhorst V, Hampton TG, Wong SL, Voorhees JR, Wagner DD (2013) Lack of tryptophan hydroxylase-1 in mice results in gait abnormalities. PLoS One 8(3):e59032

Tansey MG, McCoy MK, Frank-Cannon TC (2007) Neuroinflammatory mechanisms in Parkinson's disease: potential environmental triggers, pathways, and targets for early therapeutic intervention. Exp Neurol 208(1):1–25

Tavassoly O, Lee JS (2012) Methamphetamine binds to alpha-synuclein and causes a conformational change which can be detected by nanopore analysis. FEBS Lett 586(19):3222–3228

Thomas DM, Kuhn DM (2005) Attenuated microglial activation mediates tolerance to the neurotoxic effects of methamphetamine. J Neurochem 92(4):790–797

Thompson PM, Hayashi KM, Simon SL, Geaga JA, Hong MS, Sui Y, Lee JY, Toga AW, Ling W, London ED (2004) Structural abnormalities in the brains of human subjects who use methamphetamine. J Neurosci 24(26):6028–6036

Tieu K (2011) A guide to neurotoxic animal models of Parkinson's disease. Cold Spring Harb Perspect Med 1(1):a009316

Tillerson JL, Miller GW (2003) Grid performance test to measure behavioral impairment in the MPTP-treated-mouse model of parkinsonism. J Neurosci Methods 123(2):189–200

Vaillancourt DE, Spraker MB, Prodoehl J, Abraham I, Corcos DM, Zhou XJ, Comella CL, Little DM (2009) High-resolution diffusion tensor imaging in the substantia nigra of de novo Parkinson disease. Neurology 72(16):1378–1384

Volkow ND, Chang L, Wang GJ, Fowler JS, Franceschi D, Sedler M, Gatley SJ, Miller E, Hitzemann R, Ding YS, Logan J (2001) Loss of dopamine transporters in methamphetamine abusers recovers with protracted abstinence. J Neurosci 21(23):9414–9418

Volkow ND, Wang GJ, Smith L, Fowler JS, Telang F, Logan J, Tomasi D (2015) Recovery of dopamine transporters with methamphetamine detoxification is not linked to changes in dopamine release. Neuroimage 121:20–28

Walsh SL, Wagner GC (1992) Motor impairments after methamphetamine-induced neurotoxicity in the rat. J Pharmacol Exp Ther 263(2):617–626

Wang JJ, Lin WY, Lu CS, Weng YH, Ng SH, Wang CH, Liu HL, Hsieh RH, Wan YL, Wai YY (2011) Parkinson disease: diagnostic utility of diffusion kurtosis imaging. Radiology 261(1):210–217

Wu XF, Wang AF, Chen L, Huang EP, Xie WB, Liu C, Huang WY, Chen CX, Qiu PM, Wang HJ (2014) S-Nitrosylating protein disulphide isomerase mediates alpha-synuclein aggregation caused by methamphetamine exposure in PC12 cells. Toxicol Lett 230(1):19–27

Zhu JP, Xu W et al (2006) Methamphetamine-induced striatal apoptosis in the mouse brain: comparison of a binge to an acute bolus drug administration. Neurotoxicology 27(1):131–136